PHOTONICS Research

Arbitrary cylindrical vector beam generation enabled by polarization-selective Gouy phase shifter

Junliang Jia,[1,2,3] Kepeng Zhang,[1,3] Guangwei Hu,[2] Maping Hu,[1,3] Tong Tong,[1] Quanquan Mu,[4] Hong Gao,[3] Fuli Li,[3] Cheng-Wei Qiu,[2,5] and Pei Zhang[1,3,6]

[1]MOE Key Laboratory for Nonequilibrium Synthesis and Modulation of Condensed Matter, School of Physics, Xi'an Jiaotong University, Xi'an 710049, China
[2]Department of Electrical and Computer Engineering, National University of Singapore, Singapore, Singapore
[3]Shaanxi Key Laboratory of Quantum Information and Quantum Optoelectronic Devices, School of Physics, Xi'an Jiaotong University, Xi'an 710049, China
[4]State Key Laboratory of Applied Optics, Changchun Institute of Optics, Fine Mechanics, and Physics, Chinese Academy of Sciences, Changchun 130033, China
[5]e-mail: chengwei.qiu@nus.edu.sg
[6]e-mail: zhangpei@mail.ustc.edu.cn

Received 12 January 2021; revised 27 March 2021; accepted 29 March 2021; posted 30 March 2021 (Doc. ID 419368); published 25 May 2021

Cylindrical vector beams (CVBs), which possess polarization distribution of rotational symmetry on the transverse plane, can be developed in many optical technologies. Conventional methods to generate CVBs contain redundant interferometers or need to switch among diverse elements, thus being inconvenient in applications containing multiple CVBs. Here we provide a passive polarization-selective device to substitute interferometers and simplify generation setup. It is accomplished by reversing topological charges of orbital angular momentum based on a polarization-selective Gouy phase. In the process, tunable input light is the only condition to generate a CVB with arbitrary topological charges. To cover both azimuthal and radial parameters of CVBs, we express the mapping between scalar Laguerre–Gaussian light on a basic Poincaré sphere and CVB on a high-order Poincaré sphere. The proposed device simplifies the generation of CVBs enormously and thus has potential in integrated devices for both quantum and classic optical experiments.

https://doi.org/10.1364/PRJ.419368

1. INTRODUCTION

It is known that angular momentum of light has a spin part associated with polarization [1] and an orbital part associated with spatial distribution [2]. A cylindrical vector beam (CVB) [3–5], acting as a solution of the vectorial Helmholtz equation [6,7], combines the two parts of angular momentum. Radial polarization and azimuthal polarization are the most conspicuous CVBs. Under tight focusing [8–10], radial polarization possesses a sharper focal spot than a homogeneously polarized beam [11,12], while azimuthal polarization can be focused into a hollow spot [13]. These peculiar properties are useful for many applications, such as particle manipulation [14–18], microscopy [19–21], material processing [22–24], near-field optics [25], and nonlinear optics [26]. Recently, the degrees of freedom of CVB are extended by ray-like trajectories [27], so that CVBs also present growing potential in the area of optical encoding [28] and optical communications [29–32].

There are many methods to generate CVBs. Special intracavity resonators could directly generate CVBs from a laser when the cavity geometry is precisely controlled into a frequency-degenerate state [33–37]. Meanwhile, single-element CVB generators have been introduced to tailor Pancharatnam–Berry phases [38–41], supporting modulation of a couple of orthogonal polarization bases with conjugate phase distributions, to generate CVBs from a given basic laser mode. All of these methods need to switch in different elements to generate CVBs with different topological charges, which is inconvenient in experiments that involve multiple CVBs. For example, if there is a circumstance that requests a tunable superposition state of CVBs with arbitrary customized amplitudes on each basis, solid metasurfaces will not be satisfactory. With the same circumstance, implementations containing interferometers, where two orthogonal polarizations are modulated by spatially programmable devices individually and are then combined together [42], still work. Though ingenious devices with high robustness [43–45] are developed, their complexity of modulating two individual parts still sets them as bulky and redundant. Therefore, it is significant to create a

compact passive device to generate CVBs with arbitrary topological charges.

In this paper, we provide and demonstrate a passive device to generate CVBs with arbitrary azimuthal and radial topological charges. It is composed with a couple of polarization-selective cylindrical lenses to realize the mode-dependent π Gouy phase [46,47] in a single polarization. The device could remain unchanged no matter the topological charges of CVBs. It even adapts to generate superimposed CVBs by employing customized wavefront modulation in incident homogeneous polarizations. In physics, the device creates a robust connection between homogeneous polarizations and CVBs, where homogeneous polarizations can be marked on a basic Poincaré sphere (PS), and CVBs can be marked on a high-order Poincaré sphere (HOPS) [48]. Mapping relationships between states on the basic PS and the first-order HOPS are experimentally proved by Stokes parameters of five representative states. Petal-like intensities are also collected to verify the extensive potential for generating states on other HOPSs.

2. MAPPING THEORY

Here Laguerre–Gaussian (LG) modes, a complete set for presenting transverse modes, are expressed with complex amplitude:

$$u_{\ell,p}(r,\phi,z) = C_{|\ell|,p}(r,z)\exp(-i\ell\phi), \tag{1}$$

where r, ϕ, and z are spatial polar coordinates, ℓ and p are indices of azimuthal and radial coordinates, respectively. ℓ is an integer and p is a natural number. $C_{|\ell|,p}$ marks a coefficient related to $|\ell|$ and p, while $\exp(-i\ell\phi)$ denotes the spiral phase of wavefront, which represents the orbital angular momentum (OAM) of light with topological charge ℓ. Employing Dirac notations, OAM state is expressed with $|\ell\rangle$, and polarization is characterized with circular bases $\{|R\rangle, |L\rangle\}$. They construct direct product state

$$\begin{aligned}|\psi(2\upsilon, 2\gamma)\rangle &= (\cos\upsilon|R\rangle e^{-i\gamma} + \sin\upsilon|L\rangle e^{i\gamma}) \otimes |\ell\rangle \\ &= \cos\upsilon|\ell, R\rangle e^{-i\gamma} + \sin\upsilon|\ell, L\rangle e^{i\gamma},\end{aligned} \tag{2}$$

which can be set on the surface of a basic PS as shown in Fig. 1(a), where 2υ is a polar angle ranging in the region $(0,\pi)$, 2γ is an equator angle ranging in $(0,2\pi)$, and three spatial axes represent Stokes parameters S_1, S_2, and S_3. CVB is defined with

$$|\psi_\ell(2\upsilon, 2\gamma)\rangle = \cos\upsilon|\ell, R\rangle e^{-i\gamma} + \sin\upsilon|-\ell, L\rangle e^{i\gamma}, \tag{3}$$

which can be unified in an analytic model referred to as HOPS [48], where the simplest is first-order HOPS ($\ell = 1$), as shown in Fig. 1(b). The definition of spherical surface in Eq. (3) and the circumstance of basic PS in Eq. (2) manifest a mapping relationship where the bases change from $\{|R\rangle, |L\rangle\}$ to $\{|\ell, R\rangle, |-\ell, L\rangle\}$.

Both radial polarization and azimuthal polarization are located on the equator of first-order HOPS. Denoting $|R\rangle = (|H\rangle - i|V\rangle)/\sqrt{2}$ and $|L\rangle = (|H\rangle + i|V\rangle)/\sqrt{2}$, Eq. (3) indicates the radial vector beam is marked with $|\psi_1(\pi/2, 0)\rangle$, and the azimuthal vector beam is notated with $|\psi_1(\pi/2, \pi)\rangle$ [49]. For convenience, they are abbreviated with spherical coordinates $(\pi/2, 0)$ and $(\pi/2, \pi)$. The corresponding states with the same coordinates $(\pi/2, 0)$ and $(\pi/2, \pi)$ for basic PS are $|H\rangle$ and $|V\rangle$ polarizations, respectively. Figure 1 elucidates the connection between the basic PS and the first-order HOPS via several representative points on the sphere. Points a1–a6 selected on the surface of the basic PS as shown in Fig. 1(a) include polarization states evolving from horizontal polarization $(\pi/2, 0)$ to diagonal polarization $(\pi/2, \pi/2)$ along with the equator and then turning to a general elliptic polarization $(\pi/4, \pi/2)$ along with the longitude line. Points a1–a6 correspond to points b1–b6 at the same positions of the first-order HOPS, which represent CVBs as shown in Fig. 1(b).

3. IMPLEMENTATION

Significantly, the mapping is characterized by a polarization-selective conversion where $|\ell, L\rangle$ is converted to $|-\ell, L\rangle$ and $|\ell, R\rangle$ remains unchanged. For this reason, the device needs two functions: response of polarization and inversion of index ℓ.

Inspired by the design of the Q-plate [38], we employ liquid crystal (LC) films coated on a pair of cylindrical lenses to realize the conversion of polarization-selective response. As shown in Fig. 2(a), a polarization-selective cylindrical lens is constructed with isotropic glass lens and inhomogeneous LC film. In fabrication, plano-convex (cylindrical) isotropic glass (SiO_2)

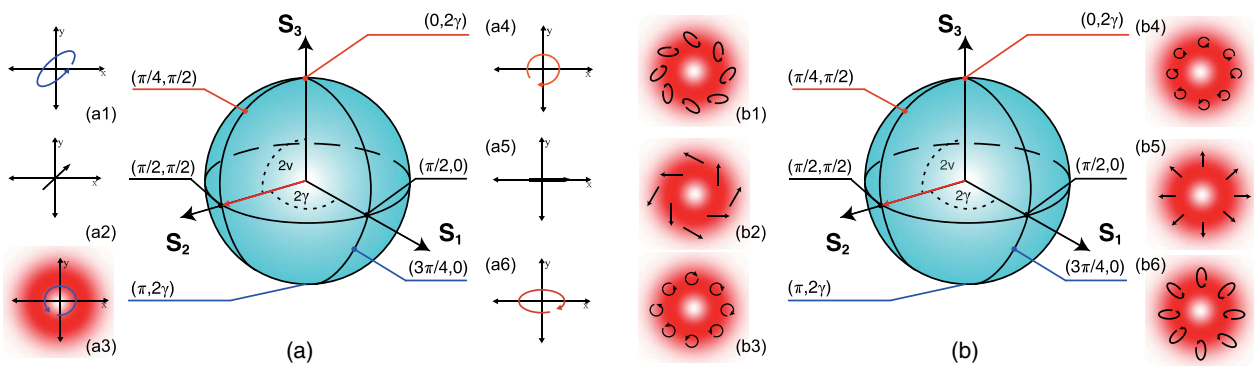

Fig. 1. (a) Basic Poincaré sphere. Selected points a1–a6 on the surface include polarization states from linear polarization to elliptical polarization. (b) First-order HOPS. Selected points b1–b6 represent six CVBs on the surface. 2υ is polar angle, and 2γ is equator angle of arbitrary state vectors directing to points on the surfaces. Points a1–a6 map b1–b6 one by one, which is just realized by the proposed device.

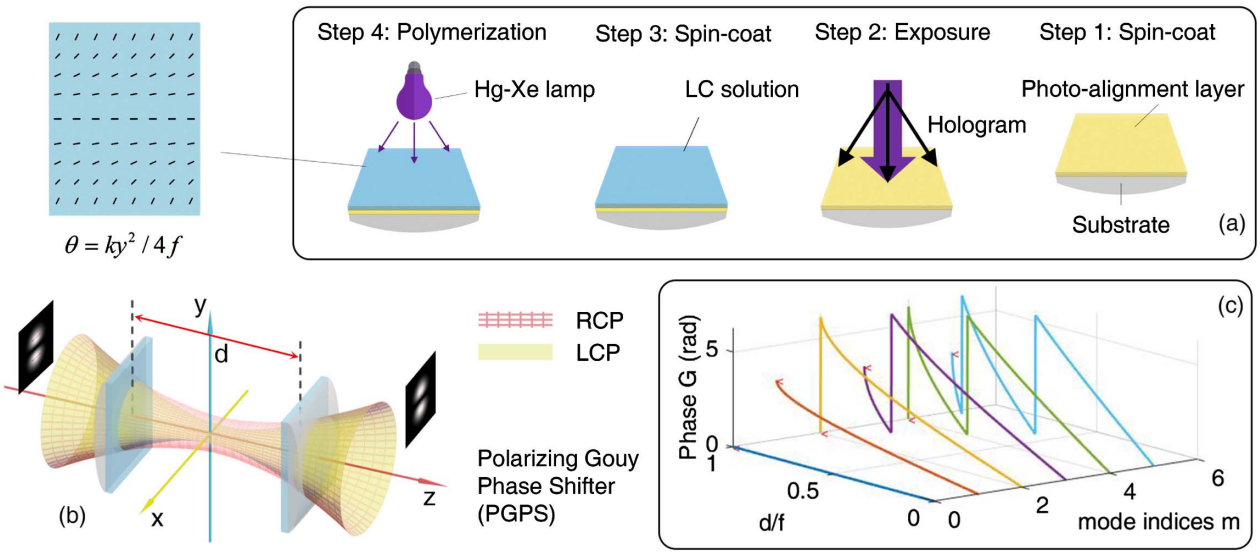

Fig. 2. (a) Fabrication of polarization-selective cylindrical lens. (b) PGPS, which contains two symmetric polarization-selective cylindrical lenses and operates on LCP only. (c) Gouy phases accumulated by PGPS for modes with different indices $m = 0$ to 5; the special points involved in the device are marked with red angles.

provides a common dynamic phase with thickness $l_0 - y^2/2f(n - n_0)$ regardless of polarization, where y is chosen as the converging direction of the cylindrical lens, n is the refractive index of the glass material, n_0 is the refractive index of air, l_0 is a constant thickness, and f is the designed focal length. The operator of the common glass lens is expressed with $\exp(+i\phi_1)(|L\rangle\langle L| + |R\rangle\langle R|)$, where $\phi_1 = -ky^2/2f$ according to Fresnel paraxial approximation. LC film is produced by four steps: (a) spin coat a photo-alignment layer onto cleaned substrate (plano-convex); (b) expose the substrate to a hologram of cylindrical wavefront implemented by a He-Cd laser beam of 325 nm wavelength; (c) spin coat LC solution onto a photo-alignment layer, which induces the alignment of LC molecules periodically under the anchoring effect; and (d) with irradiation of a mercury-xenon lamp, polymerize the LC coating under ultraviolet light. An accurate thickness with a customized focal length under 632.8 nm He–Ne laser source is obtained by multi-layer spin coating of LC solution. Thickness of LC film is mainly controlled via angular velocity of spin coating and concentration of LC solution, and then provides an extra geometric phase [50–54] by metallic distribution of fast axis angle $\theta = ky^2/4f$ related to the direction of the x axis, written with operator $\exp(-i\phi_2)|L\rangle\langle R| + \exp(+i\phi_2)|R\rangle\langle L|$, in which $\phi_2 = -ky^2/2f$. The compound operator, expressed with

$$\exp[i(\phi_1 - \phi_2)]|L\rangle\langle R| + \exp[i(\phi_1 + \phi_2)]|R\rangle\langle L| = |L\rangle\langle R| + \exp(-iky^2/f)|R\rangle\langle L|, \tag{4}$$

means a polarization-selective cylindrical lens [55] with y directional focal length $f/2$ operating on $|L\rangle$ is fabricated.

The inversion of index ℓ derives from the coefficient's conversion of Hermite–Gaussian (HG) modes. For complex amplitude of HG mode, u_{nm}^{HG}, n and m are two indices corresponding to x and y coordinates in the transverse plane. It can be seen that an LG mode, u_{nm}^{LG}, can be decomposed into a set of HG modes with the same order N ($N = n + m = 2p + |\ell|$), written as $u_{nm}^{\mathrm{LG}}(x, y, z) = \sum_{k=0}^{N} i^k b(n, m, k) u_{N-k,k}^{\mathrm{HG}}(x, y, z)$. Real coefficient $b(n, m, k)$ is given by [46]

$$b(n, m, k) = \left[\frac{(N-k)!k!}{2^N n!m!}\right]^{1/2} \frac{1}{k!}\frac{\mathrm{d}^k}{\mathrm{d}t^k}[(1-t)^n(1+t)^m]_{t=0}, \tag{5}$$

where t is a continuous parameter around the zero point. Exchanging n and m in Eq. (5), it is deduced that $b(m, n, k) = (-1)^k b(n, m, k)$. By definition $\ell = n - m$ in LG mode, extra factor $(-1)^k$ fits the conversion coefficients from ℓ to $-\ell$.

In the following, a polarization-selective device is constructed operating on HG modes (u_{nm}^{HG}), where astigmatic Gouy phase G_y is used to supply such an extra factor associated with mode index m, exactly $(-1)^m$, or written as $\exp(-imG_y)$ with $G_y = \pi$. G_y corresponds to cylindrical convergences set in the y direction. As shown in Fig. 2(b), two polarization-selective cylindrical lenses are set at the symmetrical positions relative to original point O. The condition for first piece of lens is $\phi_1 - \phi_2 = 0$, causing left-handed circular polarization (LCP) to become right-handed circular polarization (RCP) accompanied with converging effect, while RCP becomes LCP without other effect. Correspondingly, the second piece of lens, which is set in symmetrical position (flipped), turns RCP back to LCP with converging effect, such that only LCP of incident light accumulates G_y [56] between the two polarization-selective cylindrical lenses. The amount of G_y is decided by the distance between two lenses, d, and designed focal length of them, $f/2$, under proper coupling conditions. Exactly, $G_y = 2\arcsin(d/f)$, where $0 < d \le f$. The phase of wavefront performs a 2π period, so the mode-dependent phase takes effects along the instruction of $G = \mathrm{mod}(m \cdot G_y, 2\pi)$. Figure 2(c) shows amounts of G for $m = 0$ to 5 in sequence. When $d/f = 1$, special points marked with red angles perform like a phase switch between 0 and π along with the m axis, showing

factor $(-1)^m$ is attained and index ℓ becomes $-\ell$ successfully. $d/f = 1$ means $G_y = \pi$, so the device is called the π phase polarizing Gouy phase shifter (π-PGPS).

Figure 3 shows the experimental scheme. He-Ne laser derives a 632.8 nm Gaussian beam whose polarization is projected to horizontal by a half-wave plate (HWP) and a polarizing beam splitter (PBS). Two lenses constitute an expander to provide an almost plane wave for the spatial light modulator (SLM, Holoeye, Pluto-VIS-016). Fork-like holograms [57] are loaded on the screen of the SLM to produce LG modes. The beam splitter (BS) ensures light beam propagates in the correct path. Two lenses and the iris select the first order of diffracted light after the SLM by reducing them into an appropriate scale. The characteristics of the SLM determine that the original polarization of the selected beam is horizontal. If a preproduction of polarization is necessary, a quarter-wave plate (QWP) and an HWP will be included in the optical circuit. Then the π-PGPS takes effects to generate CVBs. The following QWP, HWP, PBS, and a charge-coupled device (CCD) constitute a framework to examine Stokes parameters. By changing angles of the fast axes of QWP and HWP relative to the x axis, polarizations can be reconstructed with intensities recorded by CCD. Exactly, Stokes parameters are computed via [58,59]

$$S_0 = I(0°, 0°) + I(0°, 45°), \tag{6a}$$

$$S_1 = I(0°, 0°) - I(0°, 45°), \tag{6b}$$

$$S_2 = I(45°, 22.5°) - I(45°, 67.5°), \tag{6c}$$

$$S_3 = I(45°, 0°) - I(-45°, 0°), \tag{6d}$$

where I represents collected intensities, the first angle in the parentheses is of the QWP, and the second angle is of the HWP. Results for S_0–S_3 are revealed in Fig. 4. The quality can be evaluated by comparing the outcomes computed from collected intensities with corresponding values (lower-left corner) computed from simulated intensities. Radial polarization $(\pi/2, 0)$ and azimuthal polarization $(\pi/2, \pi)$ are shown in the first two lines of Fig. 4. Original experimental pictures are collected in a relative low-intensity level in escape of overexposure of CCD, so the collections are sensitive to imperfect area of every optical element, such as SLM and PGPS. For common

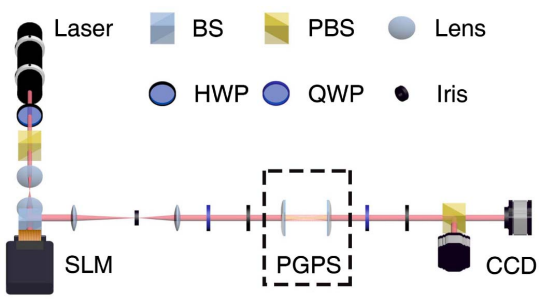

Fig. 3. Schematic of the experimental setup for generating arbitrary CVBs.

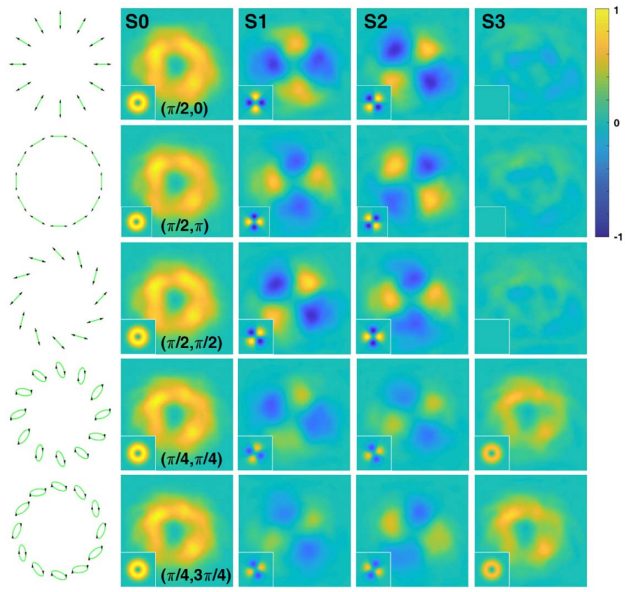

Fig. 4. Stokes parameters of CVBs. The left column displays the tailoring polarization vectors of CVBs, followed by columns of Stokes parameters S_0 to S_3. Subpictures in the lower-left corner are theoretical values. CVBs are sampled from the first-order HOPS, where $(\pi/2, 0)$, $(\pi/2, \pi)$, $(\pi/2, \pi/2)$, $(\pi/4, \pi/4)$, and $(\pi/4, 3\pi/4)$ represent their positions on the spherical surface.

instances, states marked with $(\pi/2, \pi/2)$, $(\pi/4, \pi/4)$, and $(\pi/4, 3\pi/4)$ on the first-order HOPS are presented in the last three lines. All of the experimental results agree well with the simulated values, so that the device is effective in generating CVBs on the surface of the first-order HOPS. Obviously, all elements in the installation take effects in the reverse propagation, thus proving the device constructs a credible and reversible connection between the basic PS and the first-order HOPS successfully.

As for $|\ell| > 1$, higher-order HOPSs are constructed. Representatively, a state on the equator of the HOPS can be examined by casting it into horizontal polarization via transmitted port of the PBS. The transmitted intensity performs special distribution that satisfies the petal-like shape, denoted by $I = |\langle H|\psi_\ell(\gamma, \upsilon)\rangle_p|^2$, where subscript p is the same with the index of the LG mode. Combined with Eqs. (1) and (3), it is calculated that $I = \frac{|C|^2}{2}[1 + \sin(2\upsilon)\cos(2\ell\phi + 2\gamma)]$, indicating there are $2|\ell|$ pieces of intensity petals. In other words, the number of petals can be exploited to characterize the azimuthal index ℓ of the CVB, or called the order of the HOPS. Equation (1) shows that radial index p is separated from the operation of ℓ, meaning p is an individual parameter in the construction of the HOPS. Radial index p remains unchanged, and azimuthal phase $\exp(-i\ell\phi)$ is reversed to $\exp(i\ell\phi)$ under the effect of the proposed device, so that all LG modes are connected with non-degenerated CVB completely. In notations, LG modes and CVB modes are both defined with two topological charges ℓ and p where the two indices map with the same order of each other, respectively. Expression of CVB containing p is written as

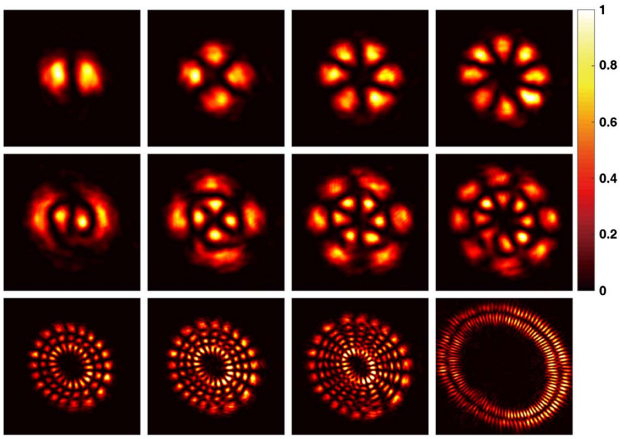

Fig. 5. Petal-like profiles collected by CCD when launching high-order LG modes. The first row is set for $p = 0$, $\ell = 1, 2, 3, 4$, and the second row is for $p = 1$, $\ell = 1, 2, 3, 4$, respectively. The third row exhibits results for $\ell = 10$, $p = 2, 3, 5$ and an ultrahigh order $\ell = 50$, $p = 1$.

$$|\psi_\ell(2\upsilon, 2\gamma)\rangle_p = \cos\upsilon|\ell, R\rangle_p e^{-i\gamma} + \sin\upsilon|-\ell, L\rangle_p e^{i\gamma}, \quad (7)$$

where $|\psi_\ell(2\upsilon, 2\gamma)\rangle_p \equiv |\psi_\ell(2\upsilon, 2\gamma)\rangle \otimes |p\rangle$. The general function of the device is illustrated by

$$\mathbb{G}|\psi(2\upsilon, 2\gamma)\rangle_p = |\psi_\ell(2\upsilon, 2\gamma)\rangle_p \quad (8)$$

containing the generation of CVB with both ℓ and p indices. $\mathbb{G}$ marks the operator of our device. In the experiment, LG modes with $\ell = 1, 2, 3, 4$ and $p = 0, 1$ are generated by the SLM. As shown in Fig. 3, removing the two HWPs and two QWPs around PGPS from the circuit, petal-like intensities are collected directly after PGPS and a PBS. In Fig. 5, the first row is set for results of $p = 0$, the second row is for $p = 1$. These pictures represent that the fabricated device is effective for CVB with both ℓ and p indices. States on other ultrahigh-order HOPS are tested by tuning $LG_{10,2}$ ($LG_{\ell,p}$), $LG_{10,3}$, $LG_{10,5}$, and $LG_{50,1}$ modes with results shown in the third line of Fig. 5. In the collected intensities, the outline of petals is always clear, showing the device works well with these higher-order CVBs.

4. CONCLUSION

We propose and demonstrate a passive device based on π-PGPS to generate arbitrary CVBs with both ℓ and p indices even in ultrahigh order. The device simplifies existing schemes for generation and builds a solid connection between a simple scalar field on the basic PS and sophisticated CVBs on the HOPS. Extensively, states on hybrid order Poincaré sphere (HyOPS) [60,61] can be implemented with the help of a spiral phase plate (SPP), which provides a shift of ℓ index of LG modes regardless of polarization. The device supplements a convenient operation for quantum information and communications experiments [62–64], taking effects on the polarization-selective mode index inversion. Generally, it can be extended to other polarization-selective converters besides $G_y = \pi$ and supports more splendid mode-dependent conversion of polarizations. The method is flexible to other techniques such as metamaterials [65–67] and metalenses [68,69], which may help to miniaturize the optical device on chips [70–72].

Funding. National Natural Science Foundation of China (11534008, 11804271, 11974345, 91736104).

Disclosures. The authors declare no conflicts of interest.

REFERENCES

1. R. A. Beth, "Mechanical detection and measurement of the angular momentum of light," Phys. Rev. **50**, 115–125 (1936).
2. L. Allen, M. W. Beijersbergen, R. Spreeuw, and J. Woerdman, "Orbital angular momentum of light and the transformation of Laguerre–Gaussian laser modes," Phys. Rev. A **45**, 8185–8189 (1992).
3. I. Freund, "Polarization flowers," Opt. Commun. **199**, 47–63 (2001).
4. Q. Zhan, "Cylindrical vector beams: from mathematical concepts to applications," Adv. Opt. Photon. **1**, 1–57 (2009).
5. X.-L. Wang, Y. Li, J. Chen, C.-S. Guo, J. Ding, and H.-T. Wang, "A new type of vector fields with hybrid states of polarization," Opt. Express **18**, 10786–10795 (2010).
6. D. G. Hall, "Vector-beam solutions of Maxwell's wave equation," Opt. Lett. **21**, 9–11 (1996).
7. X.-L. Wang, J. Ding, W.-J. Ni, C.-S. Guo, and H.-T. Wang, "Generation of arbitrary vector beams with a spatial light modulator and a common path interferometric arrangement," Opt. Lett. **32**, 3549–3551 (2007).
8. J. Pu and Z. Zhang, "Tight focusing of spirally polarized vortex beams," Opt. Laser Technol. **42**, 186–191 (2010).
9. A. P. Porfirev, A. V. Ustinov, and S. N. Khonina, "Polarization conversion when focusing cylindrically polarized vortex beams," Sci. Rep. **6**, 6 (2016).
10. E. Otte, K. Tekce, and C. Denz, "Tailored intensity landscapes by tight focusing of singular vector beams," Opt. Express **25**, 20194–20201 (2017).
11. K. S. Youngworth and T. G. Brown, "Focusing of high numerical aperture cylindrical-vector beams," Opt. Express **7**, 77–87 (2000).
12. R. Dorn, S. Quabis, and G. Leuchs, "Sharper focus for a radially polarized light beam," Phys. Rev. Lett. **91**, 233901 (2003).
13. Q. Zhan and J. R. Leger, "Focus shaping using cylindrical vector beams," Opt. Express **10**, 324–331 (2002).
14. D. G. Grier, "A revolution in optical manipulation," Nature **424**, 810–816 (2003).
15. Q. Zhan, "Trapping metallic Rayleigh particles with radial polarization," Opt. Express **12**, 3377–3382 (2004).
16. Z. Man, Z. Bai, J. Li, S. Zhang, X. Li, Y. Zhang, X. Ge, and S. Fu, "Optical cage generated by azimuthal-and radial-variant vector beams," Appl. Opt. **57**, 3592–3597 (2018).
17. A. Turpin, V. Shvedov, C. Hnatovsky, Y. V. Loiko, J. Mompart, and W. Krolikowski, "Optical vault: a reconfigurable bottle beam based on conical refraction of light," Opt. Express **21**, 26335–26340 (2013).
18. X. Weng, X. Gao, H. Guo, and S. Zhuang, "Creation of tunable multiple 3D dark spots with cylindrical vector beam," Appl. Opt. **53**, 2470–2476 (2014).
19. S. W. Hell and J. Wichmann, "Breaking the diffraction resolution limit by stimulated emission: stimulated-emission-depletion fluorescence microscopy," Opt. Lett. **19**, 780–782 (1994).
20. D. P. Biss, K. S. Youngworth, and T. G. Brown, "Dark-field imaging with cylindrical-vector beams," Appl. Opt. **45**, 470–479 (2006).
21. L. Novotny, M. Beversluis, K. Youngworth, and T. Brown, "Longitudinal field modes probed by single molecules," Phys. Rev. Lett. **86**, 5251–5254 (2001).
22. M. Kraus, M. A. Ahmed, A. Michalowski, A. Voss, R. Weber, and T. Graf, "Microdrilling in steel using ultrashort pulsed laser beams with radial and azimuthal polarization," Opt. Express **18**, 22305–22313 (2010).
23. C. Hnatovsky, V. G. Shvedov, and W. Krolikowski, "The role of light-induced nanostructures in femtosecond laser micromachining with vector and scalar pulses," Opt. Express **21**, 12651–12656 (2013).

24. J. Wang, F. Castellucci, and S. Franke-Arnold, "Vectorial light–matter interaction: exploring spatially structured complex light fields," AVS Quantum Sci. **2**, 031702 (2021).
25. A. Ciattoni, B. Crosignani, P. Di Porto, and A. Yariv, "Azimuthally polarized spatial dark solitons: exact solutions of Maxwell's equations in a Kerr medium," Phys. Rev. Lett. **94**, 073902 (2005).
26. A. Bouhelier, M. Beversluis, A. Hartschuh, and L. Novotny, "Near-field second-harmonic generation induced by local field enhancement," Phys. Rev. Lett. **90**, 013903 (2003).
27. Y. Shen, X. Yang, D. Naidoo, X. Fu, and A. Forbes, "Structured ray-wave vector vortex beams in multiple degrees of freedom from a laser," Optica **7**, 820–831 (2020).
28. G. Milione, T. A. Nguyen, J. Leach, D. A. Nolan, and R. R. Alfano, "Using the nonseparability of vector beams to encode information for optical communication," Opt. Lett. **40**, 4887–4890 (2015).
29. G. Gibson, J. Courtial, M. J. Padgett, M. Vasnetsov, V. Pas'ko, S. M. Barnett, and S. Franke-Arnold, "Free-space information transfer using light beams carrying orbital angular momentum," Opt. Express **12**, 5448–5456 (2004).
30. N. Bozinovic, Y. Yue, Y. Ren, M. Tur, P. Kristensen, H. Huang, A. E. Willner, and S. Ramachandran, "Terabit-scale orbital angular momentum mode division multiplexing in fibers," Science **340**, 1545–1548 (2013).
31. G. Milione, M. P. Lavery, H. Huang, Y. Ren, G. Xie, T. A. Nguyen, E. Karimi, L. Marrucci, D. A. Nolan, R. R. Alfano, and A. E. Willner, "4×20 gbit/s mode division multiplexing over free space using vector modes and a *q*-plate mode (de)multiplexer," Opt. Lett. **40**, 1980–1983 (2015).
32. J. Jia, Z. Chang, H. Yang, Q. Liu, F. Wang, H. Gao, F. Li, and P. Zhang, "Mode sorter designed for (de)multiplexing vector vortex modes," Appl. Opt. **58**, 7094–7099 (2019).
33. Y. Kozawa and S. Sato, "Generation of a radially polarized laser beam by use of a conical Brewster prism," Opt. Lett. **30**, 3063–3065 (2005).
34. M. A. Ahmed, A. Voss, M. M. Vogel, and T. Graf, "Multilayer polarizing grating mirror used for the generation of radial polarization in Yb:YAG thin-disk lasers," Opt. Lett. **32**, 3272–3274 (2007).
35. D. Naidoo, F. S. Roux, A. Dudley, I. Litvin, B. Piccirillo, L. Marrucci, and A. Forbes, "Controlled generation of higher-order Poincaré sphere beams from a laser," Nat. Photonics **10**, 327–332 (2016).
36. D. Wei, Y. Cheng, R. Ni, Y. Zhang, X. Hu, S. Zhu, and M. Xiao, "Generating controllable Laguerre–Gaussian laser modes through intracavity spin-orbital angular momentum conversion of light," Phys. Rev. Appl. **11**, 014038 (2019).
37. Z. Wang, Y. Shen, D. Naidoo, X. Fu, and A. Forbes, "Astigmatic hybrid SU(2) vector vortex beams: towards versatile structures in longitudinally variant polarized optics," Opt. Express **29**, 315–329 (2021).
38. L. Marrucci, C. Manzo, and D. Paparo, "Optical spin-to-orbital angular momentum conversion in inhomogeneous anisotropic media," Phys. Rev. Lett. **96**, 163905 (2006).
39. F. Cardano, E. Karimi, S. Slussarenko, L. Marrucci, C. de Lisio, and E. Santamato, "Polarization pattern of vector vortex beams generated by *q*-plates with different topological charges," Appl. Opt. **51**, C1–C6 (2012).
40. J. B. Mueller, N. A. Rubin, R. C. Devlin, B. Groever, and F. Capasso, "Metasurface polarization optics: independent phase control of arbitrary orthogonal states of polarization," Phys. Rev. Lett. **118**, 113901 (2017).
41. R. C. Devlin, A. Ambrosio, N. A. Rubin, J. B. Mueller, and F. Capasso, "Arbitrary spin-to–orbital angular momentum conversion of light," Science **358**, 896–901 (2017).
42. C. Rosales-Guzmán, N. Bhebhe, and A. Forbes, "Simultaneous generation of multiple vector beams on a single SLM," Opt. Express **25**, 25697–25706 (2017).
43. H. Chen, J. Hao, B.-F. Zhang, J. Xu, J. Ding, and H.-T. Wang, "Generation of vector beam with space-variant distribution of both polarization and phase," Opt. Lett. **36**, 3179–3181 (2011).
44. S. Chen, X. Zhou, Y. Liu, X. Ling, H. Luo, and S. Wen, "Generation of arbitrary cylindrical vector beams on the higher order Poincaré sphere," Opt. Lett. **39**, 5274–5276 (2014).
45. R. Liu, L.-J. Kong, W.-R. Qi, S.-Y. Huang, Z.-X. Wang, C. Tu, Y. Li, and H.-T. Wang, "Compact, robust, and high-efficiency generator of vector optical fields," Opt. Lett. **44**, 2382–2385 (2019).
46. M. W. Beijersbergen, L. Allen, H. Van der Veen, and J. Woerdman, "Astigmatic laser mode converters and transfer of orbital angular momentum," Opt. Commun. **96**, 123–132 (1993).
47. J. Jia, Q. Li, K. Zhang, D. Chen, C. Wang, H. Gao, F. Li, and P. Zhang, "Integrated design of $\pi/2$ converter and its experimental performance," Appl. Opt. **57**, 6076–6082 (2018).
48. G. Milione, H. Sztul, D. Nolan, and R. Alfano, "Higher-order Poincaré sphere, Stokes parameters, and the angular momentum of light," Phys. Rev. Lett. **107**, 053601 (2011).
49. A. A. Tovar, "Production and propagation of cylindrically polarized Laguerre–Gaussian laser beams," J. Opt. Soc. Am. A **15**, 2705–2711 (1998).
50. R. Simon, H. Kimble, and E. Sudarshan, "Evolving geometric phase and its dynamical manifestation as a frequency shift: an optical experiment," Phys. Rev. Lett. **61**, 19–22 (1988).
51. P. G. Kwiat and R. Y. Chiao, "Observation of a nonclassical Berry's phase for the photon," Phys. Rev. Lett. **66**, 588–591 (1991).
52. Z. Bomzon, V. Kleiner, and E. Hasman, "Pancharatnam–Berry phase in space-variant polarization-state manipulations with subwavelength gratings," Opt. Lett. **26**, 1424–1426 (2001).
53. Z. Bomzon, G. Biener, V. Kleiner, and E. Hasman, "Space-variant Pancharatnam–Berry phase optical elements with computer-generated subwavelength gratings," Opt. Lett. **27**, 1141–1143 (2002).
54. C. Oh and M. J. Escuti, "Achromatic diffraction from polarization gratings with high efficiency," Opt. Lett. **33**, 2287–2289 (2008).
55. E. Hasman, V. Kleiner, G. Biener, and A. Niv, "Polarization dependent focusing lens by use of quantized Pancharatnam–Berry phase diffractive optics," Appl. Phys. Lett. **82**, 328–330 (2003).
56. S. Feng and H. G. Winful, "Physical origin of the Gouy phase shift," Opt. Lett. **26**, 485–487 (2001).
57. E. Bolduc, N. Bent, E. Santamato, E. Karimi, and R. W. Boyd, "Exact solution to simultaneous intensity and phase encryption with a single phase-only hologram," Opt. Lett. **38**, 3546–3549 (2013).
58. B. Schaefer, E. Collett, R. Smyth, D. Barrett, and B. Fraher, "Measuring the Stokes polarization parameters," Am. J. Phys. **75**, 163–168 (2007).
59. J. Wang, X. Yang, Y. Li, Y. Chen, M. Cao, D. Wei, H. Gao, and F. Li, "Optically spatial information selection with hybridly polarized beam in atomic vapor," Photon. Res. **6**, 451–456 (2018).
60. X. Yi, Y. Liu, X. Ling, X. Zhou, Y. Ke, H. Luo, S. Wen, and D. Fan, "Hybrid-order Poincaré sphere," Phys. Rev. A **91**, 023801 (2015).
61. Z. Liu, Y. Liu, Y. Ke, Y. Liu, W. Shu, H. Luo, and S. Wen, "Generation of arbitrary vector vortex beams on hybrid-order Poincaré sphere," Photon. Res. **5**, 15–21 (2017).
62. J. Wang, J.-Y. Yang, I. M. Fazal, N. Ahmed, Y. Yan, H. Huang, Y. Ren, Y. Yue, S. Dolinar, M. Tur, and A. E. Willner, "Terabit free-space data transmission employing orbital angular momentum multiplexing," Nat. Photonics **6**, 488–496 (2012).
63. Y. Zhou, M. Mirhosseini, S. Oliver, J. Zhao, S. M. H. Rafsanjani, M. P. Lavery, A. E. Willner, and R. W. Boyd, "Using all transverse degrees of freedom in quantum communications based on a generic mode sorter," Opt. Express **27**, 10383–10394 (2019).
64. F. Wang, P. Zeng, J. Zhao, B. Braverman, Y. Zhou, M. Mirhosseini, X. Wang, H. Gao, F. Li, R. W. Boyd, and P. Zhang, "High-dimensional quantum key distribution based on mutually partially unbiased bases," Phys. Rev. A **101**, 032340 (2020).
65. D. Lin, P. Fan, E. Hasman, and M. L. Brongersma, "Dielectric gradient metasurface optical elements," Science **345**, 298–302 (2014).
66. G. Hu, X. Hong, K. Wang, J. Wu, H.-X. Xu, W. Zhao, W. Liu, S. Zhang, F. Garcia-Vidal, B. Wang, P. Lu, and C. Qiu, "Coherent steering of nonlinear chiral valley photons with a synthetic Au-WS_2 metasurface," Nat. Photonics **13**, 467–472 (2019).
67. G. Hu, M. Wang, Y. Mazor, C. Qiu, and A. Alã, "Tailoring light with layered and Moiré metasurfaces," Trends Chem. **3**, 342–358 (2021).
68. F. Aieta, P. Genevet, M. A. Kats, N. Yu, R. Blanchard, Z. Gaburro, and F. Capasso, "Aberration-free ultrathin flat lenses and axicons at telecom wavelengths based on plasmonic metasurfaces," Nano Lett. **12**, 4932–4936 (2012).

69. M. Khorasaninejad, W. T. Chen, R. C. Devlin, J. Oh, A. Y. Zhu, and F. Capasso, "Metalenses at visible wavelengths: diffraction-limited focusing and subwavelength resolution imaging," Science **352**, 1190–1194 (2016).
70. A. Y. Piggott, J. Lu, K. G. Lagoudakis, J. Petykiewicz, T. M. Babinec, and J. Vučković, "Inverse design and demonstration of a compact and broadband on-chip wavelength demultiplexer," Nat. Photonics **9**, 374–377 (2015).
71. J. Chen, X. Chen, T. Li, and S. Zhu, "On-chip detection of orbital angular momentum beam by plasmonic nanogratings," Laser Photon. Rev. **12**, 1700331 (2018).
72. K. Wei, W. Li, H. Tan, Y. Li, H. Min, W.-J. Zhang, H. Li, L. You, Z. Wang, X. Jiang, T. Chen, S. Liao, C. Peng, F. Xu, and J. Pan, "High-speed measurement-device-independent quantum key distribution with integrated silicon photonics," Phys. Rev. X **10**, 031030 (2020).